

Comparison of d -moment perturbations from hyperfine fields and neutron scattering in Fe alloys

M. B. Stearns and L. A. Feldkamp

Scientific Research Staff, Ford Motor Company, Dearborn, Michigan 48121

(Received 8 August 1974)

In the preceding paper we obtained solute- and host-moment perturbations from hyperfine-field data on dilute alloys of Fe with $3d$ and $4d$ transition atoms. Here we Fourier invert these moment perturbations to compare them with neutron diffuse-elastic-scattering curves taken on similar alloys. We find that in general the shapes of the Fourier-inverted curves agree very well with the neutron-scattering curves. In many cases the solute moments obtained from the hyperfine-field data are quite different from those determined by a previous analysis of the neutron-scattering data. We show in detail why the latter analysis led to several incorrect results. The host-moment perturbations are believed to result from the variation in the number of itinerant d electrons in the vicinity of the solute atom, as discussed in the preceding paper.

I. INTRODUCTION

In two previous papers^{1,2} (referred to as I and II), hyperfine field (hff) spectra of dilute alloys of $3d$ and $4d$ transition elements in Fe were analyzed to obtain the solute-moment and host-moment perturbations of the Fe atoms surrounding the solute atom. It was found that the host-moment perturbations can be identified as arising from the polarization induced in the itinerant d electrons by the localized d electrons, mainly via Coulomb exchange interactions, as discussed in II. Similar information is contained in data from neutron diffuse-elastic-scattering experiments on these alloys.³ Since the neutron scattering data are obtained in wave-vector space, they must be Fourier inverted to obtain the moment distributions. Such experiments are very difficult because of the small magnetic disorder cross sections of most of these alloys and the large magnetic coherent cross section of the Fe itself. This necessitated using long-wavelength neutrons (5.3 Å) in order to reduce multiple Bragg scattering, resulting in the maximum scattering vector Q being less than 1.5 \AA^{-1} . Because of this and since the neutron data have appreciable scatter, it was impossible to Fourier invert the data to obtain unique values for the moment perturbations. Therefore only rather general trends were derived from direct analysis of the neutron data. In particular, the solute-atom moment values were obtained by assuming the scattering at the largest Q values to be due solely to the solute atoms. This value was then extrapolated back to the origin using the known form factor for an atomic $3d$ -like moment distribution. We will show that this procedure is faulty. Collins and Low (CL) were aware of these difficulties and discussed them in Ref. 3, but

apparently often underestimated the errors in their procedure.

In contrast, the hff data directly give values for the solute-atom moment and the host-moment perturbations, and it is a simple matter to Fourier transform these for comparison with the neutron data. We discuss the Fourier-transformation procedure in Sec. II and compare to the neutron data in Sec. III. We show that all the features of the neutron data are well produced by the Fourier transform, thus confirming that the solute-moment and host-moment perturbations obtained from the hff data as well as the procedure and interpretation of the analysis are essentially correct. To the authors' knowledge, there has been no previous explanation for the origin of the variety of shapes observed in the neutron scattering data for Fe. The apparently simpler shapes obtained for Ni alloys^{3,4} have often been interpreted in terms of spin-dependent potentials arising from charge perturbations.⁵ This approach, however, has many shortcomings and does not give adequate fits to much of the data, as discussed in I. The nickel data are amenable also to the interpretation of arising from itinerant d electrons. However, because of the location of some of the spin-down localized states at the Fermi level in Ni, the moment decreases due to this effect appear to dominate its magnetic behavior. This is discussed in II.

II. RELATION BETWEEN NEUTRON CROSS SECTIONS AND MOMENT PERTURBATIONS

The differential cross section for diffuse elastic magnetic scattering of unpolarized neutrons from a dilute binary alloy in the form of a single-domain single crystal has been shown^{3,6} to be

$$\frac{d\sigma}{d\Omega} = \left(\frac{\gamma e^2}{2mc^2} \right)^2 \left[1 - \left(\frac{Q_z}{Q} \right)^2 \right] Nc(1-c) \times \left| \int d^3\vec{r} \rho'(\vec{r}) \exp(i\vec{Q} \cdot \vec{r}) \right|^2 \quad (1)$$

where the integral extends over the volume of the specimen and the magnetization is in the z direction. γ is the neutron gyromagnetic ratio, m is the electron mass, and $(\gamma e^2/2mc^2)^2$ has the value 0.073 b. N is the number of atoms in the crystal and c is the fractional concentration of solute atoms. For elastic scattering, the magnitude of the scattering vector \vec{Q} is given by

$$Q = (4\pi/\lambda) \sin \frac{1}{2}\Theta, \quad (2)$$

where λ is the neutron wavelength and Θ is the scattering angle. The quantity $\rho'(\vec{r})$ represents the magnetic-moment perturbation distribution caused by the addition of a single solute atom at the origin.

The experiments considered here were performed by measuring the scattering cross section with a magnetic field alternately along and perpendicular to \vec{Q} , so that the net cross section corresponds to the condition $Q_z = 0$. Further, the use of polycrystalline specimens means that the appropriate cross section is an orientation average of Eq. (1).

As discussed in II and supported by these neutron experiments, the moment contributions from the itinerant electrons have a very atomiclike spatial distribution. We therefore consider $\rho'(\vec{r})$ to be a superposition of distributions centered at atomic sites \vec{x}_i , i.e.,

$$\rho'(\vec{r}) = \sum_{i=0} \Delta_i f_i(\vec{r} - \vec{x}_i), \quad (3)$$

where Δ_i is the moment perturbation at the i th atom surrounding a solute atom at the origin ($i=0$). We assume that the alloys are sufficiently dilute that the effects due to the solute atoms are additive. $f_i(\vec{r})$ represents the volume-normalized spatial distribution of the moment perturbations. We assume, as discussed in Sec. IV of I, that the moment distributions, including that of the solute atom, are all of the same form as that of an Fe atom. For numerical calculations, their Fourier transforms can be adequately approximated by

$$F(Q) = e^{-Q^2/4b^2}, \quad (4)$$

where b^2 has been obtained from neutron form-factor measurements⁷ to be 4.7 \AA^{-2} . Thus the last factor in Eq. (1) becomes

$$\left| \int d^3\vec{r} \rho'(\vec{r}) e^{i\vec{Q} \cdot \vec{r}} \right|^2 = F(\vec{Q})^2 \left| \sum_i \Delta_i e^{i\vec{Q} \cdot \vec{x}_i} \right|^2, \quad (5)$$

where

$$F(\vec{Q}) = \int f(\vec{r}) e^{i\vec{Q} \cdot \vec{r}} d^3\vec{r}. \quad (6)$$

If the form factor $F(\vec{Q})$ is isotropic as in (4), the orientation average of (5) yields

$$\left(\frac{d\sigma}{d\Omega} \right)_{\text{polycrys.}}^{\vec{H} \perp \vec{Q}} = A F(Q)^2 \sum_{ij} \frac{\Delta_i \Delta_j \sin(Q|\vec{x}_i - \vec{x}_j|)}{Q|\vec{x}_i - \vec{x}_j|}, \quad (7)$$

the quantity $A = (\gamma e^2/2mc^2)^2 Nc(1-c)$ being constant for a given specimen.

The perturbation amplitudes Δ_i are related to the change in average moment with solute content through

$$\begin{aligned} \frac{d\bar{\mu}}{dc} &= \int d^3\vec{r} \rho'(\vec{r}) = \sum_{i=0}^{\text{max}} \Delta_i \\ &= \mu_Z - \mu_{\text{Fe}} + \sum_{i=1}^{\text{max}} \Delta_i, \end{aligned} \quad (8)$$

where μ_Z is the solute-atom moment. This is the same as Eq. (3) of II since we shall assume that all the atoms in a given shell n have the same perturbation Δ_n .

Hence at $\vec{Q} = 0$ we get

$$\left(\frac{d\sigma}{d\Omega} \right)_{\text{polycrys.}}^{\vec{H} \perp \vec{Q}} (\vec{Q} = 0) = A \left(\frac{d\bar{\mu}}{dc} \right)^2. \quad (9)$$

As CL point out, in practically all cases the $Q=0$ cross-section values inferred by extrapolating from their measurements agree very well with the values obtained from Eq. (8) when measured average saturation magnetization values are used. This indicates that the spatial distributions of the moment perturbations are indeed atomiclike. To obtain a feeling for the validity of various approximations, we show in Fig. 1 several calculations based on the Δ_i values obtained for FeNi from the hff data in I and II and listed in Table I. The solid curve is the exact expression obtained from Eq. (7), namely

$$G(Q) = F(Q)^2 \sum_{ij} \frac{\Delta_i \Delta_j \sin(Q|\vec{x}_i - \vec{x}_j|)}{Q|\vec{x}_i - \vec{x}_j|}. \quad (10)$$

For large Q the terms $i \neq j$ of Eq. (7) tend to cancel because of their rapid oscillations, giving

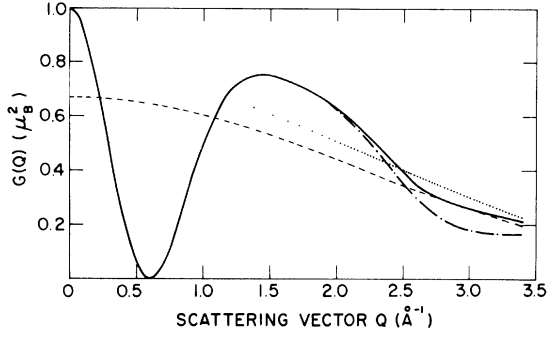


FIG. 1. Calculations of the shape of the neutron scattering as a function of scattering vector for $FeNi$ from the solute- and host-moment perturbations obtained from the hff data analysis. The solid curve is "exact," Eq. (10), the dot-dashed curve is the spherical approximation, Eq. (16), the dashed curve gives the contribution of the solute moment only, and the dotted curve is the asymptotic expression, Eq. (11), for large Q .

$$G(Q \rightarrow \infty) \approx F(Q)^2 \sum_i \Delta_i^2. \quad (11)$$

This quantity is shown as the dotted curve in Fig. 1. We see that the magnitude of Q for which this limit is approached is about 2.8 \AA^{-1} , considerably greater than the maximum Q ($\sim 1.5 \text{ \AA}^{-1}$) of the neutron experiments of Ref. 3. CL obtained the solute moment by assuming the scattering value at their highest Q was given by $F(Q)^2 \Delta_0^2$. The dashed curve shows this quantity for the Δ_0 value obtained from the hff data. We see clearly that the higher Δ_i values are still contributing appreciably at $Q \sim 1.5 \text{ \AA}^{-1}$, so that the value of Δ_0 obtained by CL is considerably too high. Since $\Delta_0 = \mu_{Ni} - \mu_{Fe}$, this then leads to a value of μ_{Ni} which is too low; CL obtained $0.9\mu_B$ as compared to the value $1.4\mu_B$ obtained from the hff data. The node in the $FeNi$ scattering data clearly comes about because the sign of the solute-moment perturbation Δ_0 is opposite to that of the total host-moment perturbation

TABLE I. Derived solute moments μ_z and host-moment perturbations Δ_n of the n th shell surrounding the solute moment.

	μ_z	Δ_1	Δ_2	Δ_3	Δ_4	Δ_5
Ni	1.4 ± 0.1	0.095	0.062	0.022	0.013	0.012
Co	1.9 ± 0.1	0.07	0.045	0.016	0.01	
Mn	1.0 ± 0.1	-0.05	-0.12	-0.025	0.016	0.016
Cr	-0.7	0.11	-0.28	0.03	0.03	0.03
	0.0	0.06	-0.27	-0.11	0.076	0.076
V	-0.2 ± 0.1	0.24	-0.38	-0.15	0.06	0.06
Rh	1.1 ± 0.2	0.11	0.073	0.026	0.016	0.014
Ru	1.0 ± 0.2	-0.0076	-0.023	0.002	0.043	0.043
Mo	0.2 ± 0.2	-0.11	-0.11	0.03	0.03	0.03

$$\Delta\mu_n = \sum_{i=1}^n \Delta_i.$$

Since Δ_0 is always negative, nodes no longer occur in the neutron scattering data when $\Delta\mu_n$ is also negative. All these features are clearly seen.

For further comparison, we reconsider Eq. (1) in the spherical approximation (SA). In the latter, an orientation average is performed on $\rho'(\vec{r})$ before the integration and squaring. This average is given by

$$\rho'(r) = \frac{1}{4\pi} \int \rho'(\vec{r}) \sin\theta d\theta d\phi, \quad (12)$$

the angles being measured from an arbitrary reference. With $\rho'(\vec{r})$ given by Eq. (3), this becomes

$$\rho'(r) = \frac{1}{4\pi} \int \sum_i \Delta_i f(\vec{r} - \vec{x}_i) \sin\theta d\theta d\phi. \quad (13)$$

Let us use the distribution corresponding to Eq. (4), namely

$$f(r) = a^3 \pi^{-3/2} e^{-b^2 r^2}, \quad (14)$$

where a is the lattice constant. The fact that $f(0) \neq 0$ as for a true d wave function emphasizes that this is not a correct form. However it is close enough, since the scattering results are relatively insensitive to the behavior of the electron wave functions very close to the nucleus. Thus we get

$$\rho'(r) = a^3 \pi^{-3/2} \sum_i \Delta_i e^{-b^2(r^2 + |\vec{x}_i|^2)} \times \cosh(2b^2 r |\vec{x}_i|), \quad (15)$$

so that

$$G(Q)_{SA} = \left(\int 4\pi r^2 dr \rho'(r) \frac{\sin Qr}{Qr} \right)^2. \quad (16)$$

The evaluation of this for $FeNi$ is shown in Fig. 1 as the dot-dashed curve. It is seen to approximate the exact expression very well out to $Q \approx 2.0 \text{ \AA}^{-1}$, beyond which it begins to break down.

III. COMPARISON WITH NEUTRON DATA

In order to compare to the neutron data, we obtained the solute moments μ_z and the host-moment perturbations Δ_n for each shell in a manner similar to that used in II. The variations consisted of taking into account that ΔH_3 was small in those cases where this information was known. Further, in the cases where we had obtained only Δ_1 , Δ_2 , and $\Delta_3 = \Delta_4 = \Delta_5$, we estimated Δ_3 and Δ_4

$=\Delta_5$ separately by drawing a smooth curve through the Δ_n values. We then took values for Δ_3 and $\Delta_4 = \Delta_5$ from this curve such that

$$\sum_{n=1}^5 M_n \Delta_n = \Delta \mu_h ,$$

where M_n is the number of atomic sites in the n th shell. The results are not altered perceptibly by reasonable variations of Δ_3 and $\Delta_4 = \Delta_5$. We set $\Delta_4 = \Delta_5$ since their shell radii are very similar and their values small. The values used are derived from set A in II and are listed in Table I and shown in Figs. 2(a) and 3(a). Using these values, we determined the quantity $G(Q)$ of Eq. (10). The errors introduced by representing the $4d$ transition element moments by a $3d$ -like form factor are discussed in Sec. II of II. The results obtained here are relatively insensitive to reasonable variations in the form factor. $G(Q)$ is shown in Figs. 2(b) and 3(b) and is to be compared to $(d\sigma/d\Omega)/Nc(1-c)$ shown in Figs. 2(c) and 3(c). We see that the main features seen in the neutron scattering data are reproduced very well. In order to see where the various features of the neutron scattering data arise, it is especially instructive to consider the spherical approximation. The advantage of this is that we can consider the transform of $\rho'(r)$ before squaring, and thus obtain separately the transform of the solute atom,

$$g_s = 4\pi \int \Delta_0 f(r) \frac{\sin Qr}{Qr} r^2 dr , \quad (17)$$

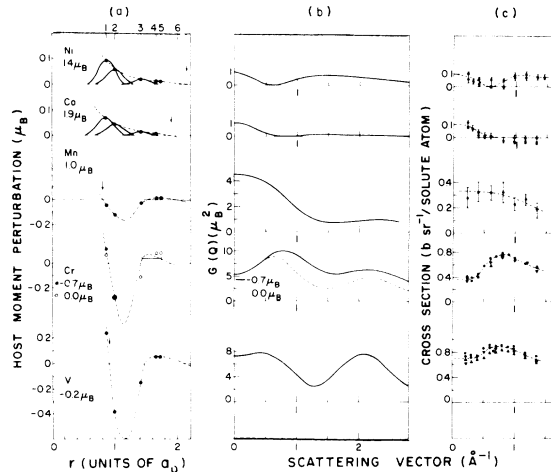


FIG. 2. (a) Host-moment perturbations surrounding $3d$ transition series solute atoms from hff data. (b) The corresponding "exact" calculated neutron scattering curves resulting from the Fourier inversion of the hff solute and host-moment perturbations. (c) The corresponding measured neutron scattering cross sections. Note that the neutron scattering data extend only to $Q \approx 1.4 \text{\AA}^{-1}$.

and that of the host moment perturbation,

$$g_h = 4\pi \int \sum_{i=1}^{i_{\max}} f(r^2 + |\vec{x}_i|^2)^{1/2} \times \cosh(2b^2 r |\vec{x}_i|) \frac{\sin Qr}{Qr} r^2 dr . \quad (18)$$

We will discuss the features of each alloy individually. We list in Table II the values of $\Delta \mu_h$ and μ_s obtained from the hff analysis in II. We also list the measured $d\bar{\mu}/dc$ and in the last column the μ_s value obtained by CL.

Ni

We see in Fig. 2 that for Ni we reproduce the node at $Q \sim 0.6 \text{\AA}^{-1}$ and the shape of the curve excellently. $G(Q)$ rises slightly beyond 1\AA^{-1} to about the same height as $Q=0$, just as the neutron scattering data does. The moment obtained in the CL analysis, $0.9 \pm 0.15 \mu_B$, is quite different from that obtained from the hff data, $1.4 \pm 0.1 \mu_B$, for the reasons discussed in Sec. II. The value of $0.9 \mu_B$ would incorrectly lead to $G(Q)$ at high Q rising to a value $\sim 70\%$ higher than the value at the origin. We show in Fig. 4 the curves of g_s , g_h , and their sum. $G(Q)$ is essentially the square of their sum for $Q \leq 2 \text{\AA}^{-1}$. We see that the node appears because $\Delta_0 = -0.8 \mu_B$ and $\Delta \mu_h = 1.8 \mu_B$, so $g_s + g_h$ passes through zero at about $Q \sim 0.6 \text{\AA}^{-1}$. Whereas g_h decreases rapidly with increasing Q , g_s falls very slowly and, since Δ_0 is an appreciable fraction of $\Delta_0 + \Delta \mu_h$, the curve rises to almost its value at the origin for higher Q values.

Co

Again we see from Fig. 2 that $G(Q)$ reproduces the neutron data very well, falling from $Q=0$ to

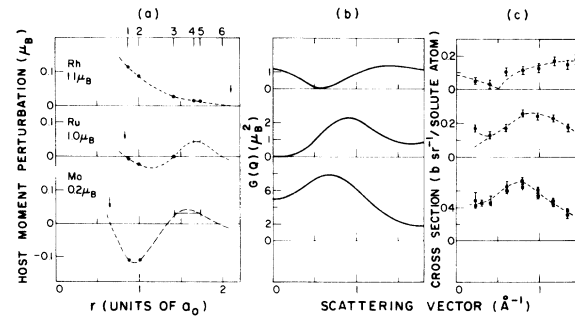


FIG. 3. (a) Host-moment perturbations surrounding $4d$ transition series solute atoms from hff data. (b) The corresponding "exact" calculated neutron scattering curves resulting from the Fourier inversion of the hff solute and host-moment perturbations. (c) The corresponding measured neutron scattering cross sections.

TABLE II. Summary of various moment quantities (in μ_B).

Solute	$d\bar{\mu}/dc$ ^a	hff $\Delta\mu_h$	hff ^a μ_z	Neutron ^b μ_z
Ni	1.0	1.8	1.4 ± 0.1	0.9 ± 0.15
Co	1.04	1.3	1.9 ± 0.1	2.1 ± 0.5
Mn	-2.1	-0.9	1.0 ± 0.2	0 ± 0.2
Cr	-2.3	-0.1 to +0.6	0.0 to -0.7 (assumed)	-0.7 ± 0.4
V	-2.69	-0.3	-0.2 ± 0.1	-0.4 ± 0.4
Rh	1.1	2.2	1.1 ± 0.1	0.5 ± 0.3
Ru	0	1.2	1.0 ± 0.1	0.9 ± 0.5
Mo	-2.2	-0.2	0.2 ± 0.2	-0.1 ± 0.6

^a See Ref. 2^b See Ref. 3.

$Q \sim 0.7 \text{ \AA}^{-1}$ and then remaining rather flat. Since in this case $\Delta_0 = -0.3\mu_B$ is small and the value at the origin comes mainly from $\Delta\mu_h (= 1.3\mu_B)$, $G(Q)$ stays very small beyond the value of the node. Incidentally, this behavior is qualitatively similar to that of all those Ni-based dilute alloys⁴ in which the solute atom has no moment. In that case $\Delta_0 = -0.6\mu_B$, whereas in general $\Delta\mu_h$ is large (and negative). Thus the neutron scattering data is expected to fall from values determined by $d\bar{\mu}/dc$ to near zero within $Q \approx 1 \text{ \AA}^{-1}$, as observed.

Mn

$G(Q)$ for Mn is seen from Fig. 2 to decrease smoothly with no node. This is because both $\Delta_0 = -1.2\mu_B$ and $\Delta\mu_h = -0.9$ are negative and thus $g_s + g_h$ never approaches zero for $Q < 1.5 \text{ \AA}^{-1}$. This can be seen in Fig. 4 for the similar situation of Mo.

This is the same general behavior as seen in the neutron scattering data, although this was interpreted in Ref. 3 to indicate that there was no moment on the Mn atom and no host perturbation in the surrounding Fe atoms. A more recent neutron scattering experiment,⁸ extending to larger Q ($\sim 2.8 \text{ \AA}^{-1}$), observed a peak in the scattering at around 2.4 \AA^{-1} , contradicting the CL interpretation. However, CL also had doubts about their interpretation since they stated that the scattering from a second Mn alloy showed traces of a maximum at $Q \neq 0$. The value of $\mu_{Mn} = 1.0 \pm 0.2\mu_B$ obtained from the hff at the solute atom is also in agreement with that obtained by analyzing the temperature dependence of the hff at the Mn atom^{9,10} and at its nearest-neighbor Fe atoms.¹⁰ We conclude that the neutron data for the FeMn alloys may not be reliable and should be repeated.

Cr

The hff at the Cr atom has not been measured and so μ_{Cr} has not been determined from hff data.

Because the neutron scattering data strongly appears to favor a negative moment, we have shown the host-moment perturbations and $G(Q)$ for both $\mu_{Cr} = -0.7\mu_B$ and $\mu_{Cr} = 0\mu_B$. We see that both show the general behavior seen in the neutron scattering data. As seen in Fig. 4 for Mo, the shape of the g_h curve can have a maximum at $Q \neq 0$ for particular Δ_n values. The value for μ_{Cr} obtained by CL

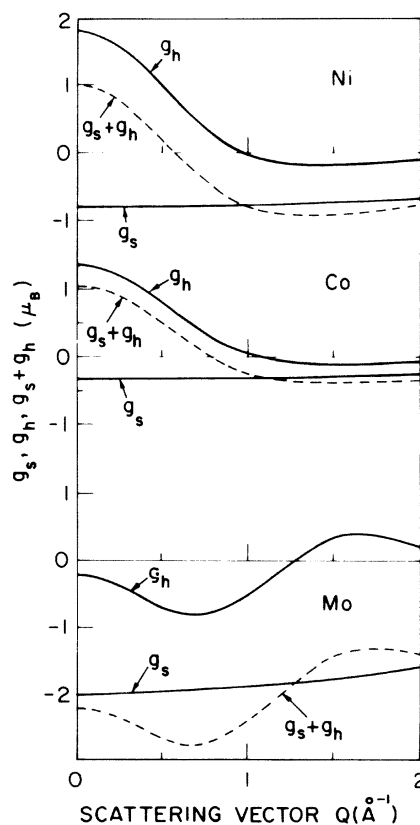


FIG. 4. Fourier transforms of the solute- (g_s) and host- (g_h) moment distributions in the spherical approximation. The square of the sum, $g_s + g_h$, gives very nearly $G(Q)$.

was $\mu_{Cr} \sim -0.7\mu_B$. However, the two solutions for the Δ_n 's proposed by CL in the second part of Ref. 3 lead to pairs of hff shifts for the first and second Fe shells surrounding a solute atom of 45 and 20 kG for the solution with $\Delta_1 = \Delta_2$ or 49 and 11 kG for the other solution. These are incompatible with the measured values of 34 and 24 kG to about ± 3 kG. A value of $\mu_{Cr} = -0.7\mu_B$ with our Δ_n values listed in Table I gives a hff at Cr of ~ -52 kG; the values for $\mu_{Cr} = 0\mu_B$ give $H_{Cr} = -110$ kG. It is clearly of interest to determine the Cr hff value experimentally; -52 kG corresponds to a resonance frequency of about 11 MHz and -110 kG to about 25 MHz. This is in a frequency range which is easily measured so the Cr hff should be attainable.

V

$G(Q)$ for V is seen to agree fairly well with that measured in the neutron scattering experiments. The moment obtained from hff data, $(-0.2 \pm 0.1)\mu_B$, agrees with that from the neutron data analysis $(-0.4 \pm 0.4)\mu_B$. In this case, $\Delta_0 = -2.4\mu_B$ and $\Delta\mu_h = -0.3\mu_B$ and the individual g_s and g_h curves are generally similar to those shown for Mo in Fig. 4. Thus the maximum at $Q \neq 0$ comes from the form of g_h .

Rh

The case of Rh is similar to that of Ni and Co in that $\Delta_0 = -1.1\mu_B$ and $\Delta\mu_h = 2.2\mu_B$ are of opposite signs and thus lead to a node. The shape of $G(Q)$ is seen to agree very well with that of the neutron scattering data. Again since Δ_0 and $\Delta\mu_h$ are both rather large, we have a case, similar to that of Ni, where the moment determined by CL has a large error. The value given by CL is $(0.5 \pm 0.3)\mu_B$, whereas that obtained from the hff fields is $(1.1 \pm 0.1)\mu_B$. As for the case of Ni, $\Delta\mu_h$ is large so that g_h contributes sufficiently at $Q \sim 1.5 \text{ \AA}^{-1}$ that extrapolation from this region yields too large a value for Δ_0 and, consequently, too small a value for μ_{Rh} .

Ru

The hff shift values for Ru are well determined and lead to knowing Δ_1 , Δ_2 , Δ_3 , and $\Delta_4 = \Delta_5$ quite accurately. Since Ru is in the same column as Fe, we expect relatively small values of Δ_n and $d\bar{\mu}/dc$. That this is so can be seen in Tables I and II. The shape of $G(Q)$ is in good agreement with that of the neutron scattering curve, except for the point at smallest Q . However, the latter is rather questionable since $d\bar{\mu}/dc$ is known to be zero with the consequence [see Eq. (9)] that the

neutron scattering curve should approach zero at $Q = 0$. Since $\Delta_0 = -1.2\mu_B$ and $\Delta\mu_h = 1.2\mu_B$ are of the same magnitude, the importance of the $\Delta\mu_h$ contribution at $Q \approx 1.5 \text{ \AA}^{-1}$ is minor so that the analysis of CL gives a moment, $(0.9 \pm 0.5)\mu_B$, which is in agreement with that from the hff data $(1.0 \pm 0.1)\mu_B$.

Mo

The hff data for this solute atom is very good and thus the shape of $G(Q)$ is in excellent agreement with the neutron scattering curve. Here we have $\Delta_0 = -2.0\mu_B$ and $\Delta\mu_h = -0.2\mu_B$. We show the g_s , g_h , and $g_s + g_h$ curves for Mo in Fig. 4. Notice that, in spite of $\Delta\mu_h$ being very small, the g_h curve can become quite large (e.g., -0.8 at $Q \sim 0.7 \text{ \AA}^{-1}$) and contribute appreciably to the total scattering curve. g_h is also seen to be appreciable at $Q \sim 1.5 \text{ \AA}^{-1}$ and beyond, so the procedure of extrapolating back from medium Q values to obtain Δ_0 is very risky. In this case, however, the moment obtained from the neutron analysis $(-0.1 \pm 0.6)\mu_B$ although very imprecise, is in agreement with the value from the hff data $(0.2 \pm 0.2)\mu_B$. We can see that this occurred because the maximum Q value measured for $FeMo$ was about 1.3 \AA^{-1} and in this region g_h fortuitously goes through a node and thus contributes little to Δ_0 .

IV. CONCLUSIONS

We have shown that in general the Fourier transformations of the solute- and host-moment perturbations in dilute alloys of $3d$ and $4d$ transition elements in Fe agree very well with the measured neutron scattering data. The solute moments obtained in the analysis of Collins and Low are sometimes quite different than those obtained from the hff data. We have discussed the origin of the errors made in CL's analysis and have shown that, correctly treated, the neutron scattering gives moments as obtained from the hff data.

The observed host-moment perturbations are believed to arise from the variation in the number of itinerant d electrons in the vicinity of the solute atom. These itinerant d electrons are polarized by the localized d electrons via Coulomb exchange and interband mixing interactions and this polarization, having a very atomlike spatial distribution when near a nucleus, produces the host moment perturbations.

- ¹M. B. Stearns, Phys. Rev. B 9, 2311 (1974), hereafter referred to as I.
- ²M. B. Stearns, preceding paper, Phys. Rev. B 13, 1183 (1976), hereafter referred to as II.
- ³M. F. Collins and G. G. Low, Proc. Phys. Soc. Lond. 86, 535 (1965); J. Phys. (Paris) 25, 596 (1964).
- ⁴J. B. Comly, T. M. Holden, and G. G. Low, J. Phys. C 1, 458 (1968).
- ⁵J. Friedel, Nuovo Cimento Suppl. 2, 287 (1958); J. Kanomori, J. Appl. Phys. 36, 929 (1965); H. Hayakawa, Prog. Theor. Phys. 37, 213 (1967); I. A. Campbell and A. A. Gomes, Proc. Phys. Soc. Lond. 91, 319 (1967).
- ⁶W. Marshall and S. Lovesey, *Theory of Thermal Neutron Scattering* (Oxford U. P., London, 1971).
- ⁷C. G. Shull and Y. Yamada, J. Phys. Soc. Jpn. Suppl. 17, 1 (1965); C. G. Shull, in *Electronic Structure and Alloy Chemistry of Transition Elements*, edited by P. A. Beck (Interscience, New York, 1963), p. 69.
- ⁸N. Kroo, L. Pal, and D. Jovic, in *Fourth IAEA Symposium on Neutron Inelastic Scattering* (IAEA, Vienna, 1968), Vol. II, p. 37.
- ⁹G. G. Low, Phys. Lett. 21, 497 (1966); D. A. Shirley, S. S. Rosenbaum, and E. Matthais, Phys. Rev. 170, 363 (1968).
- ¹⁰M. B. Stearns (unpublished).